

Supercritical fluid extraction of essential oil from chamomile flowers: modelling, and parameter estimation

Oliwer Sliczniuk^{a,*}, Pekka Oinas^a

^aAalto University, School of Chemical Engineering, Espoo, 02150, Finland

ARTICLE INFO

Keywords:

Supercritical extraction
Parameter estimation
Mathematical modelling

ABSTRACT

This study investigates the supercritical extraction process of essential oil from chamomile flowers. Essential oils of chamomile are used extensively for medicinal purposes. Many different products of chamomile have been developed, the most popular of which is in the form of herbal tea. A distributed-parameter model describes the fluid-solid extraction process. The concept of quasi-one-dimensional flow is applied to reduce the number of spatial dimensions. The flow is assumed to be uniform across any cross-section, although the area available for the fluid phase can vary along the extractor. The physical properties of the solvent are estimated based on the Peng-Robinson equation of state. Model parameters, including the partition factor, internal diffusion coefficient, axial diffusion coefficient, and decaying factor, were determined through maximum likelihood estimation based on experimental data assuming normally distributed errors. A set of laboratory experiments was performed under multiple constant operating conditions: 30 – 40°C, 100 – 200 bar, and $3.33 - 6.67 \times 10^{-5}$ kg/s.

1. Introduction

This study investigates the extraction of essential oil from chamomile flowers (*Matricaria chamomilla* L.) via supercritical fluid extraction techniques and the modelling of this process. Chamomile is a medicinal herb widely cultivated in southern and eastern Europe—such as Germany, Hungary, France, and Russia. It can be found outside of Europe in Brazil as discussed by Singh et al. [1]. This plant is distinguished by its hollow, bright gold cones, housing disc or tubular florets and surrounded by about fifteen white ray or ligulate florets. Chamomile has been used for its medicinal benefits, serving as an anti-inflammatory, antioxidant, mild astringent, and healing remedy. Chamomile's aqueous extract is widely used to calm nerves and mitigate anxiety, hysteria, nightmares, insomnia, and other sleep-related conditions, according to Srivastava [2]. Orav et al. [3] reported that oil yields from dried chamomile samples ranged from 0.7 to 6.7 mL/kg. The highest yields of essential oil, between 6.1 and 6.7 mL/kg, were derived from chamomile sourced from Latvia and Ukraine, while chamomile from Armenia exhibited a lower oil content of 0.7 mL/kg.

Evaluating the economic viability of the process is essential when choosing the suitable technology for essential oil extraction. Traditional methods, such as distillation and organic solvent extraction, are commonly employed but come with drawbacks. Distillation, for example, involves high temperatures that can lead to the thermal degradation of heat-sensitive compounds. This limitation has led to the increased popularity of alternative techniques like supercritical fluid extraction. Supercritical carbon dioxide is appealing due to its distinctive properties: it is inflammable,

non-toxic, and is non-corrosive. CO₂ is the most used supercritical fluid, sometimes modified by co-solvents such as ethanol. Supercritical fluids are capable of exhibiting both gas- and liquid-like properties, allowing for adjustable dissolving power through changes in operating conditions.

The literature offers various mathematical models to describe the extraction of valuable compounds from a biomass. Selecting a model requires a deep understanding of the physical processes, as each model is built on specific assumptions, mass transfer mechanisms and equilibrium dynamics.


The model proposed by Reverchon et al. [4] is the hot ball model, which is based on an analogy to heat transfer and describes an extraction process from solid particles. The model is based on assumptions that that particles contains low quantities of solute and solubility is not a limiting factor.

The Broken-and-Intact Cell model, proposed by Sovova [5], assumes that external surfaces of particles are mechanically disrupted, allowing the solvent's access to the solute in broken cells, while the solute in intact cells remains less accessible due to higher mass transfer resistance.

Reverchon [6] formulated a fluid-solid extraction model where the solute is treated as a single component, governed by internal mass transfer resistance and omitting the effects of external mass transfer, axial dispersion, and variations in fluid density and flow rate throughout the bed.

This work builds upon the linear kinetic model suggested by Reverchon [6], deriving fundamental governing equations to develop a comprehensive model for the chamomile oil extraction process. This model aims for control-oriented simplicity, assuming a semi-continuous operation within a cylindrical vessel. The process involves supercritical solvent being pumped through a fixed bed of finely chopped biomass to extract the solute, followed by separation of the solvent and solute in a flush drum to collect the extract. Parameters such as the pressure (P), feed flow rate (F_{in}) and inlet temperature (T_{in}) are adjustable and measurable, while the outlet temperature (T_{out}) and the

*Corresponding author

 oliwer.sliczniuk@aalto.fi (O. Sliczniuk)

ORCID(s): 0000-0003-2593-5956 (O. Sliczniuk); 0000-0002-0183-5558 (P. Oinas)

amount of product at the outlet can only be monitored. Figure 1 presents a simplified process flow diagram.

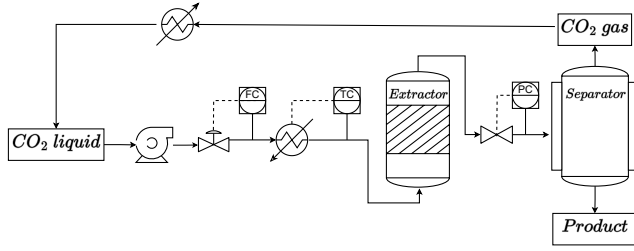


Figure 1: Process flow diagram

This study focuses on finding a process model for the extraction of natural substances from solid materials using supercritical fluids, with a particular emphasis on supercritical CO₂. The approach involves estimating the solvent properties through thermodynamic relationships and determining the extraction kinetic parameters via a series of experiments conducted under a variety of conditions. The maximum likelihood estimation method is employed solve the parameter estimation problem. Later, the correlations between parameters and operating conditions are found.

2. Materials and methods

2.1. Governing equations

Following the work of Anderson [7], the governing equations for quasi-one-dimensional were derived. Quasi-one-dimensional flow refers to a fluid flow scenario assuming that flow properties are uniformly distributed across any given cross-section. This simplification is typically applied in situations where the flow channel's cross-sectional area changes, such as through irregular shapes or partial fillings of an extractor. According to this assumption, velocity and other flow properties change solely in the flow direction.

As discussed by Anderson and Cadou [8], all flows are compressible but some of them can be treated as incompressible when the Mach number is smaller than 0.3. This assumption leads to the incompressible condition: $\nabla \cdot \mathbf{u} = 0$, which is valid for constant density (strict incompressible) or varying density flow. The restraint allows for the removal of acoustic waves, and allows for large perturbations in density and/or temperature. In the 1-D case, the incompressibility condition becomes $\frac{du}{dz} = 0$, so the fluid velocity is constant.

The set of quasi-one-dimensional governing equations in Cartesian coordinates is described by Equations 1 - 3.

$$\frac{\partial(\rho_f A_f)}{\partial t} + \frac{\partial(\rho_f A_f v)}{\partial z} = 0 \quad (1)$$

$$\frac{\partial(\rho_f v A_f)}{\partial t} + \frac{\partial(\rho_f A_f v^2)}{\partial z} = -A_f \frac{\partial P}{\partial z} \quad (2)$$

$$\frac{\partial(\rho_f e A_f)}{\partial t} + \frac{\partial(\rho_f A_f v e)}{\partial z} = -P \frac{\partial(A_f v)}{\partial z} + \frac{\partial}{\partial z} \left(k \frac{\partial T}{\partial z} \right) \quad (3)$$

where ρ_f is the density of the fluid, A_f is the function which describe change of the cross-section, v is the velocity, P is the total pressure, e is the internal energy of the fluid, t is time and z is the spacial direction.

2.2. Extraction model

2.2.1. Continuity equation

The previously derived quasi-one-dimensional continuity equation (Equation 1) is refined by incorporating a function $A_f = A\phi$. This modification accounts for the variability in the cross-sectional area available for fluid flow. Equation 4 presents this adaptation in the differential form of the continuity equation, capturing the dynamics of the flow as it responds to changes in the cross-section.

$$\frac{\partial(\rho_f \phi)}{\partial t} + \frac{\partial(\rho_f v A \phi)}{\partial z} = 0 \quad (4)$$

where A is the total cross-section of the extractor and ϕ describe porosity along the extractor.

Assuming that the mass flow rate is constant in time, the temporal derivative becomes the mass flux F , and the spatial derivative can be integrated along z as

$$\int \frac{\partial(\rho_f v A \phi)}{\partial z} dz = F \rightarrow F = \rho_f v A \phi \quad (5)$$

To simplify the system's dynamics, it is assumed that F is a control variable and affects the whole system instantaneously, which allows finding the velocity profile that satisfies mass continuity based on F , ϕ , and ρ_f .

$$v = \frac{F}{\rho_f A \phi} \quad (6)$$

Similarly, the superficial velocity might be introduced.

$$u = v \phi = \frac{F}{\rho_f A} \quad (7)$$

The fluid density ρ_f can be obtained from an equation of state (Appendix A.1) if temperature and thermodynamic pressure are known along z . The variation in fluid density may occurs due to pressure or a inlet temperature changes.

2.2.2. Mass balance for the fluid phase

This equation accounts for the movement of the pseudo-homogeneous fluid phase (Equation 8), which is constrained to the axial direction due to the quasi-one-dimensional approach that considers changes in the void fraction. It is also assumed that the thermodynamic pressure remains constant throughout the device. The analysis further simplifies the flow dynamics by disregarding the boundary layer near the extractor's inner wall, leading to a uniform velocity profile across any cross-section perpendicular to the axial direction. Given that the solute concentration in the solvent is negligible, the fluid phase is described as pseudo-homogeneous, with properties identical to the solvent itself. Thus, the mass balance equation include convection, diffusion, and kinetic terms to represent the fluid phase behaviour.

$$\frac{\partial c_f}{\partial t} + \frac{1}{\phi} \frac{\partial(c_f u)}{\partial z} = \frac{1-\phi}{\phi} r_e + \frac{1}{\phi} \frac{\partial}{\partial z} \left(D_e^M \frac{\partial c_f}{\partial z} \right) \quad (8)$$

c_f represents the concentration of solute in the fluid phase, r_e is a mass transfer kinetic term, and D_e^M is the axial diffusion coefficient.

2.2.3. Mass balance for the solid phase

The solid phase is considered to be stationary, without convection and diffusion terms in the mass balance equation (Equation 9). Therefore, the only significant term in this equation is the kinetic term (as defined in Equation 10), which connects the solid and fluid phases. The extract is represented by a single pseudo-component for simplicity.

$$\frac{\partial c_s}{\partial t} = \underbrace{r_e}_{\text{Kinetics}} \quad (9)$$

2.2.4. Kinetic term

As the solvent flows through the bed, CO₂ molecules diffuse into the pores and adsorb on the particle surface to form an external fluid film around the solid particles due to the solvent-solid matrix interactions. The dissolved solute diffuses from the particle's core through the solid-fluid interface, the pore, and the film into the bulk. Figure 2 shows the mass transfer mechanism, where the mean solute concentration in the solid phase is denoted as c_s and the equilibrium concentrations at the solid-fluid interface are denoted as c_s^* and c_p^* , respectively, for solid and fluid phases. The concentration of the solutes in the fluid phase in the center of the pore is denoted as c_p . As the solute diffuses through the pore, its concentration changes and reaches c_{pf} at the opening of the pore. Then the solute diffuses through the film around the particle and reaches bulk concentration c_f . The two-film theory describes the solid-fluid interface inside the pore. The overall mass transfer coefficient can be determined from the relationship between the solute concentration in one phase and its equilibrium concentration.

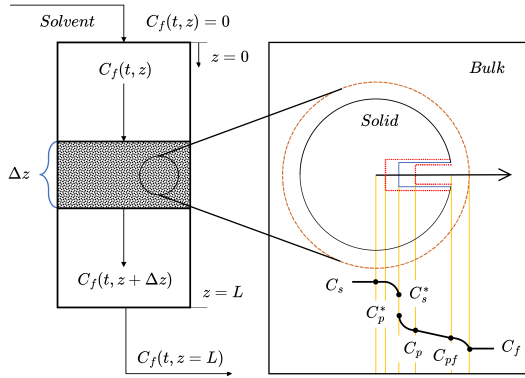


Figure 2: The mass transfer mechanism

Bulley et al. [9] suggests a process where the driving force for extraction is given by the difference between the concentration of the solute in bulk, c_f , and in the center of the pore, c_p . The concentration c_p^* is in equilibrium with c_s according to an equilibrium relationship. The rate of extraction is thus $r_e (c_f - c_p^*(c_s))$.

On the other hand, Reverchon [6] proposes a driving force given by the difference between c_s and c_p^* . c_p^* is

determined by an equilibrium relationship with c_f and the extraction rate given by Equation 10

$$r_e = \frac{D_i}{\mu l^2} (c_s - c_p^*) \quad (10)$$

where μ is sphericity, l a characteristic dimension of particles and can be defined as $l = r/3$, r is the mean particle radius, ρ_s is the solid density, D_i corresponds to the overall diffusion coefficient and c_p^* is a concentration at the solid-fluid interface (which according to the internal resistance model is supposed to be at equilibrium with the fluid phase).

According to Bulley et al. [9], a linear equilibrium relationship (Equation 11) can be used to find an equilibrium concentration of the solute in the fluid phase c_f^* is based on the concentration of the solute in the solid phase c_s .

$$c_f^* = k_p c_s \quad (11)$$

The volumetric partition coefficient k_p acts as an equilibrium constant between the solute concentration in one phase and the corresponding equilibrium concentration at the solid-fluid interphase. According to Spiro [10], k_p can be expressed through the mass partition coefficient k_m .

$$k_m = \frac{k_p \rho_s}{\rho_f} \quad (12)$$

According to Reverchon [6], the kinetic term becomes

$$r_e = -\frac{D_i}{\mu l^2} \left(c_s - \frac{\rho_s c_f}{k_m \rho_f} \right) \quad (13)$$

2.2.5. Uneven solute's distribution in the solid phase

Following the idea of the Broken-and-Intact Cell (BIC) model (Sovova [11]), the internal diffusion coefficient D_i is consider to be a product of the reference value of D_i^R and the exponential decay function γ , as given by Equation 14.

$$D_i = D_i^R \gamma(c_s) = D_i^R \exp \left(\gamma \left(1 - \frac{c_s}{c_{s0}} \right) \right) \quad (14)$$

where the γ describe the curvature of the decay function. Equation 15 describes the final form of the kinetic term

$$r_e = -\frac{D_i^R \gamma}{\mu l^2} \left(c_s - \frac{\rho_s c_f}{k_m \rho_f} \right) \quad (15)$$

Such a formulation limits the availability of the solute in the solid phase. Similarly to the BIC model, if solute is assumed to be contained in the cells, a part of which is open because the cell walls were broken by grinding, and the rest remains intact. The diffusion of the solute from a particle's core takes more time compared to the diffusion of the solute located close to the outer surface. Considering that the internal diffusion coefficient decay as the concentration of the solute in the solid decrease. As the value of the c_s decrease over time, the exponential term approach unity and $\lim_{c_s \rightarrow 0} D_i = D_i^R$. D_i^R can be interpreted as the internal diffusion coefficient at vanishing gradient.

Alternatively, the decay function γ can be consider with respect to the Shrinking Core model presented by Goto et al. [12], where the particle radius change as the amount of solute in the solid phase decrease. As the particle size decrease

due to dissolution, the diffusion path increase which makes the diffusion slower and reduce the value of a diffusion coefficient. The same analogy can be apply to the Equation 14 to explain the change of the diffusion coefficient.

2.2.6. Extraction yield

The process yield is calculated according to Equation 16 as presented by Sovova et al. [13]. The measurement equation evaluates the solute's mass at the extraction unit's outlet and sums it up. The integral form of the measurement (Equation 16) can be transformed into the differential form (Equation 17) and augmented with the process model.

$$y = \int_{t_0}^{t_f} \frac{F}{\rho_f} c_f \Big|_{z=L} dt \quad (16)$$

$$\frac{dy}{dt} = \frac{F}{\rho_f} c_f \Big|_{z=L} \quad (17)$$

2.2.7. Initial and boundary conditions

It is assumed that the solvent is free of solute at the entrance of the extractor and that all the solid particles have the same initial solute content c_{s0} . As the residence time is much shorter than the sampling time, the initial state estimate for the concentration of the solute in the fluid phase would be not reliable. Considering that it is assumed that the $c_{f0} = 0$ and that the system is isothermal. Therefore, the initial and boundary conditions are define as follow:

$$\begin{aligned} c_f(t=0, z) &= 0 & c_s(t=0, z) &= c_{s0} & c_f(t, z=0) &= 0 \\ \frac{\partial c_f(t, z=L)}{\partial x} &= 0 & c_s(t, z=\{0, L\}) &= 0 & y(0) &= 0 \end{aligned}$$

2.2.8. Discretization methods

The method of lines is used to transform the process model equations into a set of ODEs denoted as $G(x; \Theta)$. The backward finite difference is used to approximate the first-order derivative, while the central difference scheme is used to approximate the second-order derivative z -direction. The length of the fixed bed is divided into N_z equally distributed points in z -direction. The state-space model after the discretization is represented by x .

$$\dot{x} = \frac{dx}{dt} = \begin{bmatrix} \frac{dc_{f,1}}{dt} \\ \vdots \\ \frac{dc_{f,N_z}}{dt} \\ \frac{dc_{s,1}}{dt} \\ \vdots \\ \frac{dc_{s,N_z}}{dt} \\ \frac{dy(t)}{dt} \end{bmatrix} = \begin{bmatrix} G_1(c_f, c_s; \Theta) \\ \vdots \\ G_{N_z}(c_f, c_s; \Theta) \\ \vdots \\ G_{2N_z}(c_f, c_s; \Theta) \\ \vdots \\ G_{2N_z+2}(c_f, c_s; \Theta) \end{bmatrix} \underbrace{\quad}_{G(x; \Theta)}$$

where $x \in \mathbb{R}^{N_x=2N_z+1}$ and $\Theta \in \mathbb{R}^{N_\Theta=N_\theta+N_u}$, N_θ is the number of parameters, N_u is the number of control variables.

For a derivative to be conservative, it must form a telescoping series. In other words, after the addition of all

terms coming from the discretization over a grid, only the boundary terms should remain, and the artificial interior points should cancel out. The discretization is applied to the conservative form of the model to ensure mass conservation.

2.3. Parameter estimation

Only some of the parameters in a process model can be estimated from the theoretical considerations. The goal of parameter estimation is to obtain the "best" estimate of unknown parameters θ (which is a subset of the parameter space Θ containing all parameters of a model) based on the continuous observations $Y(t)$ or the discrete observations $Y(t_i)$. Conceptually, the unobservable error $\epsilon(t)$ is added to the deterministic model output, $y(t)$ (Equation 16), to give the observable dependent variable $Y(t)$ (for example results of an experiment). For discrete observations, this can be expressed as:

$$Y(t_i) = y(\theta, t_i) + \epsilon(t_i)$$

For continuous variables, the equation is:

$$Y(t) = y(\theta, t) + \epsilon(t)$$

However, obtaining analytical solutions for a deterministic process model can be challenging, so experiments are often conducted where the vector of derivatives $dY(t_i)/dt$ is measured instead of $Y(t_i)$ itself. In such cases, it is assumed that the unobservable error is added to the deterministic derivative $dy(\theta, t_i)/dt$ as shown below

$$\frac{dY(t_i)}{dt} = \frac{dy(\theta, t_i)}{dt} + \epsilon(t_i) \quad (18)$$

In the case where the error in the first observation is denoted as ϵ_1 , the error in the second observation ϵ'_2 incorporates ϵ_1 as well as an independent random component, given by $\epsilon'_2 = \epsilon_1 + \epsilon_2$. Similarly, the error in the third observation is $\epsilon'_3 = \epsilon_1 + \epsilon_2 + \epsilon_3$, etc. Mandel [14] made a distinction between the typically assumed independent measurement error in the dependent variable and a "cumulative" or interval error, in which each new observation encompasses the error of the previous ones. Cumulative errors arise from fluctuations in the process due to small variations in operating conditions and are not independent; only the differences in measurement from one period to the next are independent.

Maximum likelihood estimation (MLE) is a statistical method used to estimate the parameters of a probability distribution based on observed data. The MLE works by finding the values of the parameters that maximize the likelihood function, which is the probability of observing the given data for a given set of parameter values. The MLE has desirable properties such as asymptotic efficiency and normality. Although the MLE has often been associated with the normal distribution for mathematical convenience, it can be applied to a wide range of probability distributions. The derivation of the likelihood function under the assumption of the Gaussian distribution is discussed by Himmelblau [15]. The objective function is presented by Equation 19:

$$\ln L = -\frac{n}{2} \ln(2\pi\sigma^2) - \frac{\sum_{i=1}^n \left[\frac{dY(t_i)}{dt} - \frac{dy(\theta, t_i)}{dt} \right]^2}{2\sigma^2} \quad (19)$$

The parameter estimation problem can be formulated as follow:

$$\begin{aligned} \hat{\theta}_{MLE} &= \arg \max_{\sigma, \theta \in \Theta} \ln L = \arg \max_{\sigma, \theta \in \Theta} p(\theta|y) \\ \text{subject to} \quad &\dot{x} = G(x(t); \theta) \\ &\dot{\theta} = 0 \\ &y = y(t) \\ &\theta^{lb} \leq \theta \leq \theta^{ub} \end{aligned} \quad (20)$$

where $\hat{\theta}$ is as maximum likelihood estimator, θ^{lb} define the minimal value of θ , θ^{ub} is the maximum value of θ and σ represents the standard deviation of the residuals (errors) between the observed data points and the model outputs.

The initial guess for each decision variable, as well as the lower and upper bounds are given in Table 1.

Parameter	k_m [-]	$D_i^R \times 10^{-13} [m^2/s]$	$D_e^M \times 10^{-12} [m^2/s]$	Y [-]
Lower bound	0	0	0	0
Upper bound	$+\infty$	$+\infty$	$+\infty$	$+\infty$
Initial guesses	0.1-10	0.1 – 10	0.1-10	0.1-10

Table 1: Constraints and initial guess

Solution of Equations 20 yield the desired estimates $\hat{\theta}$. For some models, these equations can be explicitly solved for $\hat{\theta}$ but in general, no closed-form solution to the maximization problem is known or available, and a maximum likelihood estimator can only be found via numerical optimization.

2.4. Experimental work

In order to solve the optimization problem presented by Equation 20, it is necessary to calibrate the model based on the experimental the dataset $Y(t)$, which was obtained by extracting oil from chamomile flowers. The experiments were performed by Povh et al. [16] and Rahimi et al. [17]. The experiments were conducted using an a semi-batch extractor with diameter of 3.96 [cm] and length of 16.55 [cm]. Twelve experiments were performed under different operating conditions: 30 – 40°C, 100 – 200 [bar], and 0.05 – 0.24 [kg/h]. The amount of solid material used for extraction was 75 [g], which was sufficient to fill the whole vessel. The bulk density of the bed was computed based on the feed's mass and the extractor's volume. The total porosity of the bed, including the particles, was determined using the following calculation: $\epsilon = 1 - \frac{d_a}{d_r} = 1 - \frac{370}{1364} = 0.73$.

3. Results

To solve the parameter estimation problem, the single shooting method was used to transform the boundary-value problem into the initial value problem and to formulate the non-linear programming problem. This non-linear optimization task was tackled using the CasADi framework (Andersson et al. [18]). Each time series was fitted separately to the model with the linear extraction kinetics (Equation 13). The initial value problem was solved multiple times with varying initial guesses to identify the global minimum. Within the model context characterized by linear kinetics,

two parameters remain to be determined: the partition coefficient k_m and the internal diffusion coefficient D_i .

Figure 3a shows the parameter space and corresponding values of the cost function for experiment 1 (40°C, 100 bar and 6.67×10^{-5} kg/s). As the cost function is to be minimized, the lowest value of $-\ln(L)$ indicate the best fit. A black vertical stripe at $D_i \approx 0.2$ can be observed. That stripe indicates the existence of the optimal value of the D_i . In the direction of k_m , the cost function is almost flat, which suggests that any value of k_m above 0.1 fits the data equally well. If k_m can be an arbitrary point, then it can grow to infinity, which suggests that the solvent is far from the saturation, and the model can be simplified. The model reduction can be introduced by considering the limit of k_m in the extraction kinetic term:

$$\begin{aligned} \lim_{k_m \rightarrow \infty} \left(c_s(t, z) - \frac{\rho_s}{k_m(T(t, z), P(t)) \rho(T(t, z), P(t))} c_f \right) &= \\ = \left(c_s(t, z) - \frac{\rho_s}{\infty \cdot \rho(T(t, z), P(t))} c_f(t, z) \right) &= (c_s(t, z) - 0) \end{aligned}$$

The extraction model can be adapted to incorporate adjustments for the reduced kinetic term and axial diffusion. In this revised setup, two parameters remain undetermined: the internal diffusion coefficient D_i and the axial diffusion coefficient D_e^M . Figure 3b illustrates the parameter space and associated cost function values.

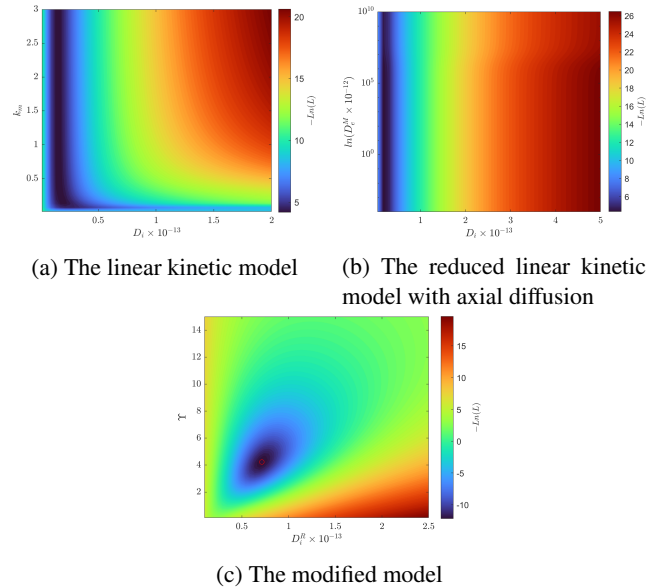


Figure 3: Parameter space for experiment 1

Similarly to the previous case, the optimal value of D_i exists, but a unique value for the D_e^M cannot be determined. Figure 3b illustrates the minimal impact of the axial diffusion coefficient, where a broad range of D_e^M yields identical cost function values. By selecting a low value D_e^M , the axial diffusion terms can be reduced or eliminated from the model without compromising its generality. This observation aligns with the findings of Rahimi et al. [17], who analysed the same dataset and reported Peclet numbers ranging between

290 and 400. Such high values of the Peclet number suggest that the advection term dominates the mass transfer, and the axial diffusion is negligible.

In both scenarios previously discussed, the fitting outcomes were not deemed satisfactory. Building upon the concepts underlying the Broken-and-Intact and Shrinking Core models (detailed in Chapter 2.2.5), the gamma function is introduced to capture the decreasing extraction kinetics. The correction factor is combined with the simplified linear model, resulting in a two-parameter model (D_i^R and Υ) as given by Equation 15. Figure 3c shows the parameter space and the corresponding cost function values.

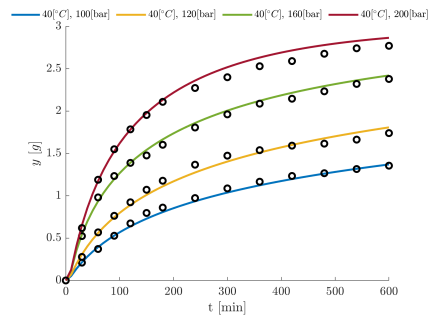
The parameter space for the revised model exhibits a distinct minimum value corresponding to the solution of the parameter estimation problem for experiment 1. The red circle highlights the minimum value of the cost function found by the optimizer. The remaining experiments are fitted to the modified extraction model, and results are presented in Figure 4. The obtained results show good agreement with experimental data.

The parameter estimation results are combined to analyse the relationship between the obtained parameters and the operating conditions. Unlike traditional methods that employ a combination of Reynolds, Schmidt, and Sherwood numbers to find correlations—omitted here due to the insignificance of axial diffusion—the approach in this study leverages the Reynolds number ($Re = \frac{(2r) \cdot \rho_f \cdot u}{\mu}$) as the sole independent variable. Using the Reynolds number has the advantage of considering the influence of all the control variables (temperature, pressure and flow rate), which means it can be uniquely defined by selecting operating conditions.

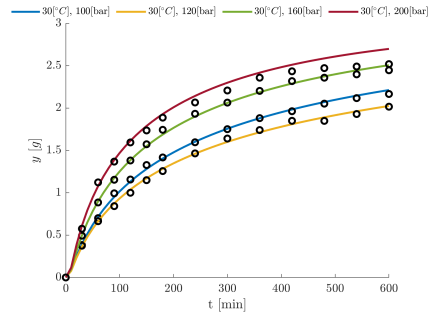
In Figures 5a and 5b, two distinct data clusters emerge, each corresponding to a different mass flow rate. Despite the linear trends observed in both sets of correlations, the correlations for D_i^R exhibit a decline with increasing Re , whereas those for Υ show an upward trend with Re . The decrease in D_i^R across each data line can be attributed to higher fluid density and increased mass transfer resistance.

A more general relationship can be obtained by applying multiple linear regression instead of linear regression. The clusters in Figure 5a and 5b are close to parallel, suggesting that a plane would combine all the data points. The Reynolds number and flow rate act as independent variables for D_i^R and Υ as presented in Figures 5c and 5d. The presented correlations are valid in the whole range of investigated operating conditions.

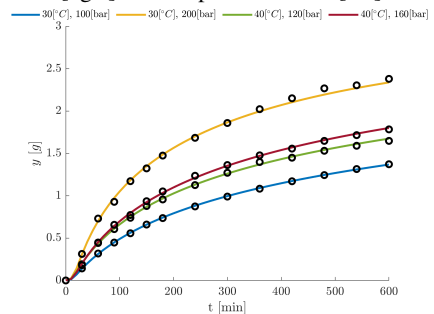
The correlations are later used against the original dataset to show that the correlations can reproduce the results with satisfactory accuracy. Figure 6 shows the results of the simulations with incorporated correlations. A good agreement between simulation results and the dataset can be observed. If Figures 4 and 6 are compared, a decrease in the accuracy of simulations can be observed. Such a behaviour is expected due the bias–variance trade-off, which describes the relationship between a model’s complexity and the accuracy of its predictions.



(a) Parameter estimation results at 6.67×10^{-5} [kg/s] and temperature of 40 [°C]



(b) Parameter estimation results at 6.67×10^{-5} [kg/s] and temperature of 30 [°C]



(c) Results of parameter estimation for experiments at 3.33×10^{-5} [kg/s]

Figure 4: Parameter estimation results

The parameter estimation results are compared against those presented by Povh et al. [16], who applied the Sovova model to the same dataset. It is important to note that Povh et al. [16] use as the initial solute mass ratio a value of 10% above the total amount of extract for every experimental, while in this work, the initial conditions are the same for all the experiments. In contrast to this work, Povh et al. [16] did not utilize numerical solvers but used a mix of analytical methodologies and trial-and-error procedures. Povh et al. [16] remarked that ‘the direct fitting of experimental data to the Sovova’s model produced parameters that could not be accepted after a careful physical interpretation of the system’. The parameters identified in this study seem to have a physical interpretation and are within the expected range.

Rahimi et al. [17] analysed the same dataset using the desorption–dissolution–diffusion model. To decrease the number of unknown parameters, Rahimi et al. [17] applied a set of empirical correlations. The remaining parameters

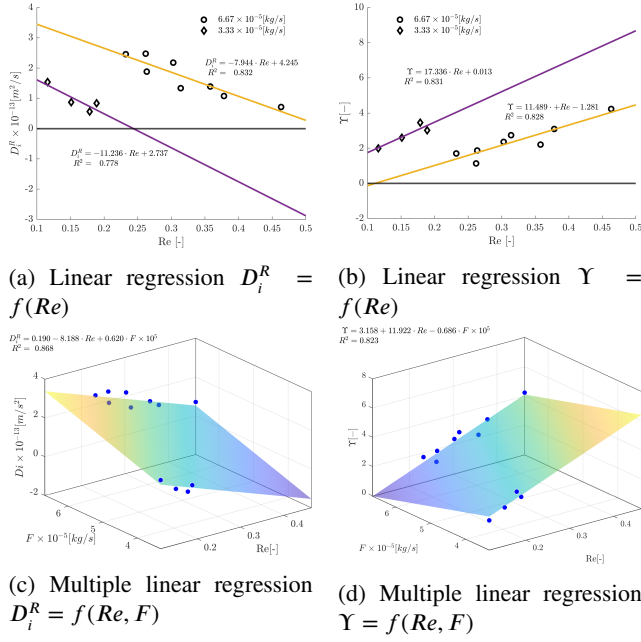


Figure 5: Parameter estimation results

were determined through the use of a genetic algorithm to solve the parameter estimation problem for each experiment individually. Results obtained by Rahimi et al. [17] shows that the desorption–dissolution–diffusion model fails to reproduce the yield data. The main difference between the model employed by Rahimi et al. [17] and the one in this study is the γ function. The γ function increases the model's flexibility by adjusting D_i and allows it to obtain a better fit.

Povh et al. [16] and Rahimi et al. [17] delivered a set of independent parameters for every single experiment. This work combines the parameters obtained from each experiment to get a single correlation valid for the whole range of investigated operating conditions.

4. Conclusions

The article presents a comprehensive study on supercritical fluid extraction of essential oil from chamomile flowers, focusing on developing and applying a distributed-parameter model to describe the fluid-solid extraction process. By employing the concept of quasi-one-dimensional flow, the study simplifies the spatial dimensions of the extraction process, ensuring uniform flow across any cross-section while allowing for variations in the area available for the fluid phase. The physical properties of the solvent are estimated using the Peng-Robinson equation of state, and key model parameters are determined through maximum likelihood estimation based on experimental data, considering normally distributed errors.

Laboratory experiments were conducted by Povh et al. [16] under various conditions to validate the model. The model parameters, such as partition factor, internal diffusion coefficient, axial diffusion coefficient, and decaying factor, were determined through maximum likelihood estimation

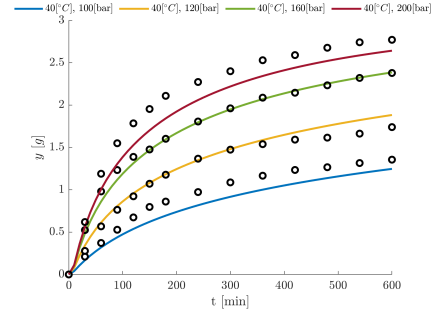
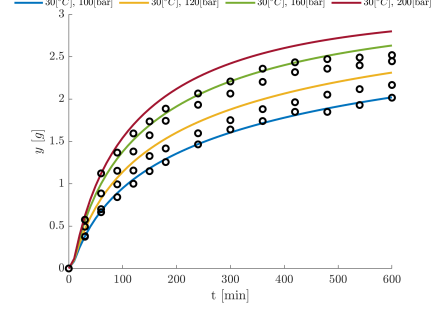
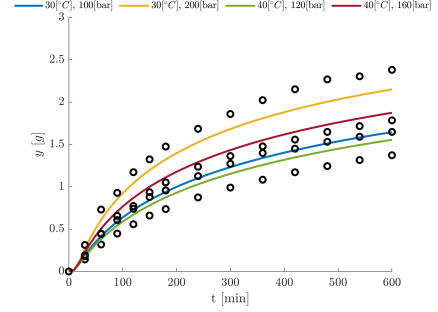

 (a) Parameter estimation results at 6.67×10^{-5} [kg/s] and temperature of 40 [°C]

 (b) Parameter estimation results at 6.67×10^{-5} [kg/s] and temperature of 30 [°C]

 (c) Results of parameter estimation for experiments at 3.33×10^{-5} [kg/s]

Figure 6: Parameter estimation results

based on experimental data. The parameter space exploration revealed that while some parameters could be determined with a high degree of confidence, others, like the axial diffusion coefficient, had a low impact on the model's output. The identification of the low-impact parameters leads to model reduction

This work introduced a set of correlations to find a general relationship between parameters and the independent variables, which can be determined by operating conditions. The obtained correlations were introduced into the model and tested against the dataset. The results show good agreement between the simulation results and all the data points.

The presented model can be further used with the presented correlations to introduce an extraction model with dynamically changing operating conditions for multiple purposes, such as yield maximisation, techno-economic analysis, or optimal experiments design.

References

- [1] Ompal Singh, Zakia Khanam, Neelam Misra, and ManojKumar Srivastava. Chamomile (*matricaria chamomilla* L.): An overview. *Pharmacognosy Reviews*, 5(9):82, 2011. ISSN 0973-7847. doi: 10.4103/0973-7847.79103.
- [2] Janmejai Srivastava. Extraction, characterization, stability and biological activity of flavonoids isolated from chamomile flowers. *Molecular and Cellular Pharmacology*, 1(3):138–147, August 2009. ISSN 1938-1247. doi: 10.4255/mcpharmacol.09.18.
- [3] Anne Orav, Ain Raal, and Elmar Arak. Content and composition of the essential oil of *chamomilla recutita* (L.) rauschert from some european countries. *Natural Product Research*, 24(1):48–55, January 2010. ISSN 1478-6427. doi: 10.1080/14786410802560690.
- [4] Ernesto Reverchon, Giorgio Donsi, and Libero Sesti Osseo. Modeling of supercritical fluid extraction from herbaceous matrices. *Industrial & Engineering Chemistry Research*, 32(11):2721–2726, nov 1993. doi: 10.1021/ie00023a039.
- [5] Helena Sovova. Rate of the vegetable oil extraction with supercritical co₂. modelling of extraction curves. *Chemical Engineering Science*, 49(3):409–414, 1994. doi: 10.1016/0009-2509(94)87012-8.
- [6] Ernesto Reverchon. Mathematical modeling of supercritical extraction of sage oil. *AIChE Journal*, 42(6):1765–1771, jun 1996. doi: 10.1002/aic.690420627.
- [7] John D. Anderson. *Computational fluid dynamics the basic with applications*. McGraw-Hill, 1995. ISBN 9780071132107.
- [8] Jr. Anderson, John D. and Chris Cadou. *Fundamentals of Aerodynamics*. McGraw-Hill Education, 2023. ISBN 9781264151929.
- [9] N. R. Bulley, M. Fattori, A. Meisen, and L. Moyls. Supercritical fluid extraction of vegetable oil seeds. *Journal of the American Oil Chemists' Society*, 61(8):1362–1365, aug 1984. doi: 10.1007/bf02542243.
- [10] M. Spiro. Extraction of ginger rhizome: partition constants and other equilibrium properties in organic solvents and in supercritical carbon dioxide. *International Journal of Food Science & Technology*, 25(5): 566–575, jun 2007. doi: 10.1111/j.1365-2621.1990.tb01116.x.
- [11] Helena Sovova. Broken-and-intact cell model for supercritical fluid extraction: Its origin and limits. *The Journal of Supercritical Fluids*, 129:3–8, nov 2017. doi: 10.1016/j.supflu.2017.02.014.
- [12] Motonobu Goto, Bhupesh C. Roy, and Tsutomu Hirose. Shrinking-core leaching model for supercritical-fluid extraction. *The Journal of Supercritical Fluids*, 9(2):128–133, jun 1996. doi: 10.1016/s0896-8446(96)90009-1.
- [13] Helena Sovova, Radko Komers, J. Kucuera, and Jaromir Jez. Supercritical carbon dioxide extraction of caraway essential oil. *Chemical Engineering Science*, 49(15):2499–2505, aug 1994. doi: 10.1016/0009-2509(94)e0058-x.
- [14] John Mandel. Fitting a straight line to certain types of cumulative data. *Journal of the American Statistical Association*, 52(280):552–566, dec 1957. doi: 10.1080/01621459.1957.10501413.
- [15] David Mautner Himmelblau. *Process analysis by statistical methods*, 1970. [by] David M. Himmelblau., Includes bibliographical references.
- [16] Nanci P. Povh, Marcia O.M. Marques, and M. Angela A. Meireles. Supercritical co₂ extraction of essential oil and oleoresin from chamomile (*chamomilla recutita* [L.] rauschert). *The Journal of Supercritical Fluids*, 21(3):245–256, November 2001. ISSN 0896-8446. doi: 10.1016/s0896-8446(01)00096-1.
- [17] E. Rahimi, J.M. Prado, G. Zahedi, and M.A.A. Meireles. Chamomile extraction with supercritical carbon dioxide: Mathematical modeling and optimization. *The Journal of Supercritical Fluids*, 56(1):80–88, February 2011. ISSN 0896-8446. doi: 10.1016/j.supflu.2010.11.008.
- [18] Joel A. E. Andersson, Joris Gillis, Greg Horn, James B. Rawlings, and Moritz Diehl. CasADi: a software framework for nonlinear optimization and optimal control. *Mathematical Programming Computation*, 11(1):1–36, jul 2018. doi: 10.1007/s12532-018-0139-4.
- [19] Ding-Yu Peng and Donald B. Robinson. A new two-constant equation of state. *Industrial & Engineering Chemistry Fundamentals*, 15(1): 59–64, feb 1976. doi: 10.1021/i160057a011.
- [20] Jürgen Gmehling, Michael Kleiber, Bärbel Kolbe, and Jürgen Rarey. *Chemical Thermodynamics for Process Simulation*. Wiley, mar 2019. doi: 10.1002/9783527809479.

A. Appendix

A.1. Thermodynamic

A.1.1. Equation of state

A cubic equation of state (EoS) serves as a mathematical model to describe the behavior of real gases and liquids through a third-degree polynomial equation that correlates the pressure, volume, and temperature of a substance. These equations constitute tools for comprehending the phase behavior, properties, and thermodynamic processes of actual substances, across various engineering and scientific applications. The cubic equation of state take into account deviations from ideal gas behavior, which are particularly important at high pressures and low temperatures, where real gases do not follow assumption of ideal gas.

$$P = \frac{RT}{v_m - b} - \frac{\Phi}{v_m^2 - uv_m + wb^2} \quad (21)$$

In this equation, P denotes the pressure of the substance, v_m represents the molar volume of the substance, T stands for the absolute temperature of the substance, u and w are integers that vary from one equation to another, R symbolizes the universal gas constant and ω denotes an acentric factor and $\Phi = a\alpha$.

The Van der Waals constants, constitute empirical values contingent upon the particular substance being modeled. These constants factor in molecular interactions (represented by 'a') and the finite size of gas molecules (indicated by 'b').

Several variations of the cubic equation of state exist, each with its own set of parameters and assumptions. Tables 2 and 3 show parameters for popular cubic EoS.

EoS	u	w	a	b
van der Waals	0	0	$\frac{27}{64} \frac{R^2 T_c^2}{P_c}$	$\frac{RT_c}{8P_c}$
Redlich and Kwong	1	0	$0.42748 \frac{R^2 T_c^{2.5}}{P_c}$	$\frac{0.08664 RT_c}{P_c}$
Soave	1	0	$0.42748 \frac{R^2 T_c^2}{P_c}$	$\frac{0.08664 RT_c}{P_c}$
Peng and Robinson [19]	2	-1	$0.45724 \frac{R^2 T_c^2}{P_c}$	$\frac{0.07780 T_c}{P_c}$

Table 2: Parameters for Popular Cubic EoS

EoS	α	$f(\omega)$
van der Waals	$\frac{1}{\sqrt{T_r}}$	-
Redlich and Kwong	$\frac{1}{\sqrt{T_r}}$	-
Soave	$\left[1 + f(\omega) \left(1 - \sqrt{T_r}\right)\right]^2$	$0.48 + 1.574\omega - 0.176\omega^2$
Peng and Robinson ([19])	$\left[1 + f(\omega) \left(1 - \sqrt{T_r}\right)\right]^2$	$0.37464 + 1.54226\omega - 0.26992\omega^2$

Table 3: Parameters for Popular Cubic EoS

The general cubic equation of state can be represented as a polynomial, as indicated in Equation 22. In a one-phase region, the fluid is characterized by a single real root, corresponding to the gas, liquid, or supercritical phase. In the two-phase region, a gas-liquid mixture exists, and two roots are identified. The larger root corresponds to the gas phase, while the smaller root pertains to the liquid phase.

$$Z^3 - (1 + B - uB)Z^2 + (A + wB^2 - uB - uB^2)Z - AB - wB^2 - wB^3 = 0 \quad (22)$$

$$\text{where } A = \frac{\Phi P}{R^2 T^2} \text{ and } B = \frac{bP}{RT}.$$

If the Peng-Robinson equation of state (Peng and Robinson [19]) is used, the polynomial equation becomes

$$Z^3 - (1 - B)Z^2 + (A - 2B - 3B^2)Z - (AB - B^2 - B^3) = 0 \quad (23)$$

For an ideal gas, the compressibility factor is defined as $Z = 1$, but the deviation of Z needs to be consider for real-life cases. The value of Z typically increases with pressure and decreases with temperature. At elevated pressures, molecules collide more frequently, allowing repulsive forces between molecules to influence the molar volume of the real gas (v_m) to surpass that of the corresponding ideal gas ($(v_m)_{ideal\ gas} = \frac{RT}{P}$), resulting in Z exceeding one. At lower pressures, molecules move freely, with attractive forces predominating, leading to $Z < 1$.

Numerical methods such as Newton-Raphson can be used to solve the polynomial equation to obtain the compressibility $Z(T(t, z), P(t))$ at given temperature and pressure. Alternatively, the closed form solution can be obtained by Cardano formula (Appendix A.2).

A.1.2. Density of the fluid phase

The density of the fluid can be calculated from the real gas equation $\rho = \frac{P}{RTZ} \frac{1}{m_{CO2}}$. The temperature can be obtain from the time evolution of governing equations, the pressure is consider to be constant along the system to be a know.

A.2. Cardano's Formula

Following the work of Gmehling et al. [20], a cubic equation of state can be written a following form

$$Z^3 + UZ^2 + SZ + T = 0 \quad (24)$$

with Z as the compressibility factor. Using Cardano's formula, this type of equation can be solved analytically.

$$P = \frac{3S - U^2}{3} \quad Q = \frac{2U^3}{27} - \frac{US}{3} + T$$

the discriminant can be determined to be

$$D = \left(\frac{P}{3}\right)^3 + \left(\frac{Q}{2}\right)^2 \quad (25)$$

For $D > 0$, the equation of state has one real solution:

$$Z = \left[\sqrt{D} - \frac{Q}{2}\right]^{1/3} - \frac{P}{3\left[\sqrt{D} - \frac{Q}{2}\right]^{1/3}} - \frac{U}{3} \quad (26)$$

For $D < 0$, there are three real solutions:

$$\Theta = \sqrt{-\frac{P^3}{27}} \quad \Phi = \arccos\left(\frac{-Q}{2\Theta}\right)$$

they can be written as

$$Z_1 = 2\Theta^{1/3} \cos\left(\frac{\Phi}{3}\right) - \frac{U}{3} \quad (27)$$

$$Z_2 = 2\Theta^{1/3} \cos\left(\frac{\Phi}{3} + \frac{2\pi}{3}\right) - \frac{U}{3} \quad (28)$$

$$Z_3 = 2\Theta^{1/3} \cos\left(\frac{\Phi}{3} + \frac{4\pi}{3}\right) - \frac{U}{3} \quad (29)$$

The largest and the smallest of the three values correspond to the vapor and to the liquid solutions, respectively. The middle one has no physical meaning.